

Thermal Atomic Layer Etching of Zinc Oxide from 30–300 °C Using Sequential Exposures of Hydrogen Fluoride and Trimethylgallium

Taewook Nam,^{||} David R. Zywojtko,^{||} Troy A. Colleran, Jonathan L. Partridge, and Steven M. George*



Cite This: *Chem. Mater.* 2025, 37, 2844–2854



Read Online

ACCESS |



Metrics & More

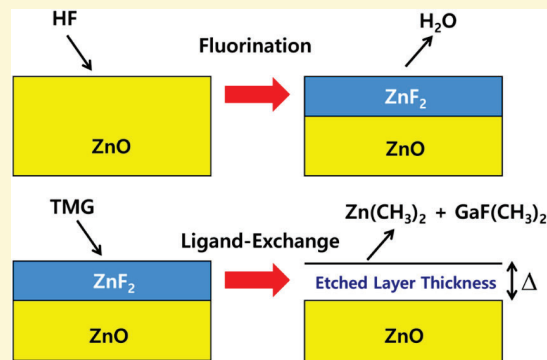


Article Recommendations



Supporting Information

ABSTRACT: Thermal atomic layer etching (ALE) of zinc oxide (ZnO) was demonstrated over a large temperature range from 30–300 °C using sequential exposures of HF (hydrogen fluoride) and Ga(CH₃)₃ (trimethylgallium (TMG)). In contrast to earlier studies of thermal ZnO ALE using sequential exposures of HF and trimethylaluminum (TMA), ZnO ALE with sequential HF and TMG exposures occurred without competing GaF₃ atomic layer deposition (ALD) or ZnO conversion. Quartz crystal microbalance (QCM) studies during ZnO ALE revealed a stepwise mass increase during fluorination by HF exposures and a larger mass decrease during ligand-exchange by TMG exposures. The mass changes per cycle (MCPC) were self-limiting versus HF and TMG exposures at 100 °C. Spectroscopic ellipsometry measured etch rates over a wide temperature range. The etch rates varied from 0.24 Å/cycle at 30 °C to 3.82 Å/cycle at 300 °C. The temperature-dependent etch rates were consistent with an activation barrier of $E_a = 3.3$ kcal/mol. TMG exposures were also compared with TMA exposures at 100 °C on fresh ZnO surfaces grown by ZnO ALD. TMG exposures led to a mass gain consistent with TMG adsorption. In contrast, TMA exposures produced a mass loss consistent with the conversion of ZnO to Al₂O₃. Previous studies showed that conversion of ZnO to Al₂O₃ prevented ZnO ALE using HF and TMA exposures at temperatures less than 205 °C. Etching at <205 °C was restricted because HF adsorption on fluorinated Al₂O₃ led to competing AlF₃ ALD. In contrast, ZnO ALE at temperatures as low as 30 °C is possible because no competing GaF₃ ALD occurs using HF and TMG exposures. Quadrupole mass spectrometry (QMS) experiments were also performed to identify the etch products during ZnO ALE. The QMS experiments support fluorination and ligand-exchange reactions without conversion during ZnO ALE using HF and TMG exposures. The HF and TMG exposures were selective for ZnO ALE compared with HfO₂, ZrO₂ or Al₂O₃ ALE. ZnO ALE could also smooth ZnO surfaces progressively versus number of ZnO ALE cycles.



Other mechanisms for thermal ALE are based on conversion reactions.^{2,12} During conversion, reactive metal precursors convert the surface of the starting material to a different material.¹² For example, boron trichloride (BCl₃) converts tungsten oxide (WO₃) to boron oxide (B₂O₃) during W and WO₃ ALE.¹³ In situ Fourier transform infrared (FTIR) and quadrupole mass spectrometry (QMS) studies also observed the conversion of Al₂O₃ to B₂O₃ by BCl₃.¹⁴ In addition, a recent study on ZnS ALE showed that zinc sulfide (ZnS) was converted to Al₂S₃ by reaction with TMA.¹⁵ ZnO ALE using HF and TMA was also observed to follow a conversion mechanism.^{12,16} The conversion involved the reaction of TMA with ZnO to form Al₂O₃. This conversion

I. INTRODUCTION

Atomic layer etching (ALE) is based on sequential, self-limiting surface modification and volatile release reactions.^{1–4} The two general types of ALE are plasma ALE and thermal ALE. Plasma ALE utilizes energetic particle bombardment to release the surface modified layer.³ In contrast, thermal ALE employs thermal reactions that volatilize the surface modified layer.^{2,5} Plasma ALE is anisotropic and is critical for forming high aspect ratio vias and trenches.³ Thermal ALE is isotropic and can provide conformal and lateral etching necessary for fabricating complex, three-dimensional structures.^{2,5}

Several different mechanisms have been developed for thermal ALE. One main mechanism is based on fluorination and ligand-exchange reactions.^{2,4} The thermal ALE of Al₂O₃ using hydrogen fluoride (HF) and trimethylaluminum (Al(CH₃)₃) (TMA) follows this mechanism.^{6,7} HF fluorinates the surface of Al₂O₃ to form AlF₃.^{6,8} Subsequently, TMA reacts with the AlF₃ surface layer and forms volatile AlF(CH₃)_x products.^{9–11} The thickness of the Al₂O₃ film decreases progressively with sequential HF and TMA exposures.^{6,7}

Other mechanisms for thermal ALE are based on conversion reactions.^{2,12} During conversion, reactive metal precursors convert the surface of the starting material to a different material.¹² For example, boron trichloride (BCl₃) converts tungsten oxide (WO₃) to boron oxide (B₂O₃) during W and WO₃ ALE.¹³ In situ Fourier transform infrared (FTIR) and quadrupole mass spectrometry (QMS) studies also observed the conversion of Al₂O₃ to B₂O₃ by BCl₃.¹⁴ In addition, a recent study on ZnS ALE showed that zinc sulfide (ZnS) was converted to Al₂S₃ by reaction with TMA.¹⁵

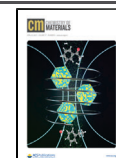
ZnO ALE using HF and TMA was also observed to follow a conversion mechanism.^{12,16} The conversion involved the reaction of TMA with ZnO to form Al₂O₃. This conversion

Received: January 4, 2025

Revised: March 11, 2025

Accepted: March 12, 2025

Published: March 31, 2025



reaction occurred because Al_2O_3 is a more stable metal oxide than ZnO . The conversion of ZnO to Al_2O_3 by TMA can be expressed as



This reaction has a very favorable predicted standard Gibbs free energy change of $\Delta G^\circ = -334.35$ kcal/mol at 100 °C.¹⁷

One possible concern with thermal ALE based on conversion reactions is that undesired metal elements from the conversion may be left behind as impurities after the ALE process. Therefore, other thermal ALE pathways for ZnO ALE that do not involve conversion reactions are desirable. These other possible thermal ALE processes may also offer a wider temperature range compared with ZnO ALE using sequential HF and TMA exposures that requires temperatures ≥ 205 °C. One alternative process for ZnO ALE can be performed at temperatures as low as 100 °C utilizing sequential H₂ and O_2 plasma exposures.¹⁸

Trimethylgallium (TMG) is a Group III precursor similar to TMA. Because of its high vapor pressure, TMG has been widely used for gallium arsenide (GaAs) or gallium nitride (GaN) synthesis by molecular beam epitaxy or metal–organic chemical vapor deposition.^{19,20} Similar to the volatile CH_3 -containing etch products generated by TMA reactions,^{9,10} CH_3 -containing etch products from TMG ligand-exchange reactions would have high volatility. TMG has been used previously as a ligand-exchange reactant.²¹ The thermal ALE of Ga_2O_3 was achieved using HF for fluorination and TMG for ligand-exchange.²¹ Ga_2O_3 thermal ALE was also demonstrated using HF for fluorination and tris(dimethylamido)gallium for ligand exchange.²² In addition, conversion reactions with metal oxides are less likely with TMG compared with TMA because Ga_2O_3 is less stable than Al_2O_3 . Density functional theory calculations also reveal that TMA has a higher conversion ability than TMG during the atomic layer deposition (ALD) of ternary Group 13 oxides.²³

The conversion of the ZnO surface to Ga_2O_3 is not expected to occur with TMG because this reaction is not thermochemically favorable. The conversion of ZnO to Ga_2O_3 by TMG can be written as



This reaction has an unfavorable predicted standard Gibbs free energy change of $\Delta G^\circ = +148.67$ kcal/mol at 100 °C.¹⁷ Consequently, TMG may be successful as a ligand-exchange precursor for ZnO ALE without causing ZnO conversion to Ga_2O_3 .

In this paper, thermal ZnO ALE was demonstrated using HF and TMG as the reactants. The etch rates of ZnO ALE were characterized using in situ quartz crystal microbalance (QCM), spectroscopic ellipsometry (SE), and X-ray reflectivity (XRR) measurements. In situ QMS studies identified the volatile species that were produced during the sequential HF and TMG exposures to ZnO powder. QCM studies also explored the differences between TMG and TMA exposures on fresh ZnO surfaces. In addition, X-ray photoelectron spectroscopy (XPS) analysis measured the residues left after ZnO ALE using HF and either TMG or TMA.

II. EXPERIMENTAL SECTION

II.I. Reactor and Reactants. The thermal ALE experiments were conducted in several hot wall reactors. The configurations of these reactors are similar to reactors that have been reported previ-

ously.^{15,24,25} For the QCM measurements, two tube reactors were connected in parallel to a precursor manifold to perform experiments at two temperatures simultaneously. The reactor chambers were enclosed in ceramic heaters (VS102A06S, VS102A12S, Watlow) to maintain the process temperature.

To achieve precise QCM measurements, the temperatures of the reactors were controlled using proportional-integral-derivative (PID) temperature controllers (Nanodac, Eurotherm) and power controllers (Epack, Eurotherm). These controllers maintained the reactor temperature within a range of ± 0.1 °C. The reactors were pumped with mechanical rotary vane pumps (2010C1, Pfeiffer). The base pressure of the reactors was maintained at 20 mTorr without any processing gas flow and ~ 1 Torr with a constant flow of ultrahigh purity grade nitrogen (N_2) gas (99.999%, Airgas).

The ZnO ALD films used for the ZnO ALE experiments were grown on a gold-coated quartz crystal (TAN06RCGP, Phillips Technologies) and p-type silicon (Si) wafer (Silicon Valley Microelectronics, Inc.) at 100 °C. The precursors for ZnO ALD were diethylzinc (DEZ) (≥ 52 wt %, Millipore Sigma) and deionized water (H_2O) (HPLC grade, Fisher Scientific). The detailed growth parameters for ZnO ALD have been reported in earlier studies.¹⁶

For ZnO ALE, HF derived from HF-pyridine (HF ~ 70 wt %, Millipore Sigma) and TMG (99.9999%, Strem) were used as the reactants. Freeze–pump–thaw cycles were used to eliminate dissolved gases from the HF-pyridine and TMG precursors. The ALD and ALE precursors were maintained at room temperature at ~ 25 °C. The HF exposures were defined by a pressure of 200 mTorr for 1 s. The TMG exposures were characterized by a pressure of 300 mTorr for 2 s. Before loading into the reactor, the Si samples were rinsed sequentially by acetone, isopropanol (IPA), and deionized water to remove surface contaminants.

II.II. QCM, SE, XRR, AFM and XPS Measurements. The mass change of ZnO films during ALE was monitored using two in situ QCM sensors.²⁴ Each QCM crystal was mounted inside a housing (CDS-A1F47-15, Inficon). The sensor housing was sealed using a low-outgassing, high temperature epoxy (Epo-Tek H21D, Epoxy Technology, Inc.) and cured at ~ 60 °C for >12 h. All of the QCM measurements were recorded by high-resolution thin film deposition monitors (SQM-160-H-2-E, Inficon). The thickness resolution of the QCM monitors was ~ 0.037 Å.

A spectroscopic ellipsometer (M-2000UI, J.A. Woollam) was utilized for monitoring the film thickness. The wavelength range for the ellipsometric measurements was from 245 to 1690 nm. The data acquisition was performed for 10 s after every reactant exposure. For the refractive index measurements, ex situ ellipsometric measurements were conducted on an automated stage by varying the incident angle from 65 to 75°. After data acquisition, the thickness and refractive index of the ZnO films were determined using the CompleteEASE software package (J.A. Woollam).

Ex situ SE measurements of ZnO , Al_2O_3 , ZrO_2 , and HfO_2 etching using sequential HF and TMG exposures were also conducted at 100 °C. These experiments were performed under identical reaction conditions to compare the etch rates. The ZrO_2 and HfO_2 films were grown using ALD methods and provided by the TEL Technology Center, America. These films were deposited at 250 °C as described earlier.²⁶ The Al_2O_3 films were deposited using ALD with sequential TMA and H_2O exposures at 225 °C.

XRR was also conducted to measure the film thickness using an X-ray diffractometer (Bede D1, Jordan Valley Semiconductors). The XRR measurements employed radiation from a $\text{Cu K}\alpha$ source at $\lambda = 1.54$ Å. The X-ray tube filament voltage and current were 40 kV and 35 mA, respectively. After measurement, the film thickness was derived using the REFS software suite (Jordan Valley Semiconductor).

Surface roughness analysis of the ZnO film deposited on a Si coupon substrate, both before and after ZnO ALE, was conducted using an atomic force microscope (AFM) (NX-10, Park Systems). The AFM operated in noncontact mode (NCM) with a scan rate of 1 Hz, utilizing a stage-mounted PPP-NCHR probe (Nanosensors).

Following image acquisition, XEI software (Park Systems) was employed to extract various parameters from the AFM images.

XPS was performed for the quantification of residual elements after ALE using a PHI 5600 (Physical Electronics) XPS system with an Al K α source (1486.6 eV). Survey scans were collected with a pass energy of 93.9 eV and a step size of 0.4 eV without Ar⁺ ion sputtering. All XPS spectra were calibrated using the C 1s XPS peak at 284.6 eV.²⁷ Peak analysis was conducted using CasaXPS (Casa Software). The data fitting employed Shirley backgrounds and Gaussian–Lorentzian functions.²⁸

II.III. QMS Studies. The QMS studies were performed in a custom-built reactor using ZnO powder samples. A detailed description of this reactor has been given previously.^{10,25} The two reactant lines were isolated until the reactants arrived at the ZnO powder sample.²⁵ The ZnO powder (>99.9%, average particle size: 80–200 nm, US Research Nanomaterials, Inc.) was housed in a stainless-steel mesh enclosure. The etching of the ZnO powder was conducted at 100 °C. The ZnO powder was placed in the reactor for at least 12 h prior to the reactant exposures to allow removal of adsorbed water from the ZnO powder.

The volatile etch products were formed in a N₂ background gas at a pressure of ~1.5 Torr in the sample holder. The partial pressure of each reactant was approximately 1 Torr. The N₂, reactant and product gases expanded through an aperture into a low pressure differentially pumped region to form a molecular beam.¹⁰ The products in the molecular beam then passed through a skimmer into a second differentially pumped region that housed the quadrupole mass spectrometer (Extrel, MAX-QMS Flanged Mounted System).¹⁰ An electron ionization energy of 70 eV was used for the QMS experiments. To minimize exposures to corrosive gases, the ionizer and analyzer were positioned perpendicular to the incoming molecular beam.

III. RESULTS AND DISCUSSION

III.I. In Situ QCM Measurements. Figure 1 shows the mass change during 50 ALE cycles on a ZnO-deposited QCM

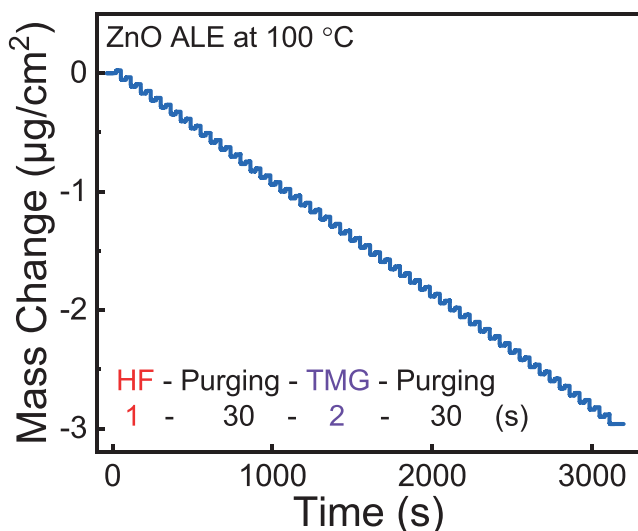


Figure 1. Mass change versus time for ZnO ALE using sequential exposures of HF and TMG at 100 °C.

crystal using sequential exposures of HF and TMG at 100 °C. The HF and TMG exposure times were 1 and 2 s, respectively, and the purging time was 30 s. Figure 1 displays a linear mass decrease versus time. The slope of the mass change versus time yields a mass change per cycle (MCPC) of $-58 \text{ ng}/(\text{cm}^2 \text{ cycle})$. This MCPC is equivalent to an etch rate of $1.04 \text{ Å}/\text{cycle}$ based on the measured ZnO ALD film density of $5.6 \text{ g}/$

cm^3 determined by XRR. In addition, the immediate mass decrease beginning with the first ALE cycle also indicates no etching delay for ZnO ALE using HF and TMG.

Figure 2 shows an enlargement of the mass change versus time for four ALE cycles shown in Figure 1. The mass changes

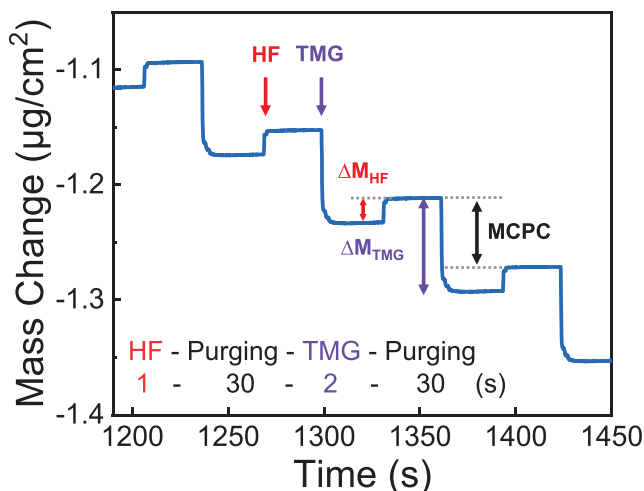
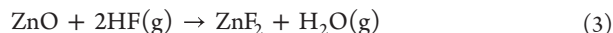


Figure 2. Enlargement of mass change for ZnO ALE at 100 °C shown in Figure 1.

for the individual HF and TMG exposures are denoted ΔM_{HF} and ΔM_{TMG} , respectively. The QCM measurements observed digital mass changes during the sequential HF and TMG exposures. Pronounced mass gains during HF exposures are monitored with a mass change of $\Delta M_{\text{HF}} = +22 \text{ ng}/(\text{cm}^2 \text{ cycle})$. Distinct mass losses are observed during TMG exposures with a mass change of $\Delta M_{\text{TMG}} = -80 \text{ ng}/(\text{cm}^2 \text{ cycle})$.

Mass increases during HF exposures are expected from fluorination of the ZnO surface to ZnF₂. The fluorination reaction for ZnO ALE can be expressed as



The fluorination reaction should be thermochemically favorable at 100 °C because the predicted standard Gibbs Free Energy is $\Delta G^\circ = -63.5 \text{ kcal}/\text{mol}$.¹⁷ From eq 3, the net mass increase for the fluorination reaction is 22 amu. Consequently, the measured mass increase of $\Delta M_{\text{HF}} = +22 \text{ ng}/(\text{cm}^2 \text{ cycle})$ is equivalent to $6.04 \times 10^{14} \text{ ZnF}_2 \text{ units}/\text{cm}^2$. Based on the ZnF₂ molar mass of 103.9 g/mol and the ZnF₂ density of 4.95 g/cm³, these $6.04 \times 10^{14} \text{ ZnF}_2 \text{ units}/\text{cm}^2$ represent a ZnF₂ thickness of 2.09 Å formed on the ZnO surface.

Mass decreases during TMG exposures are anticipated because of the removal of the ZnF₂ surface layer by the ligand-exchange reaction. The ligand-exchange reaction can be written as



This ligand-exchange reaction will be supported later by QMS studies. From eq 4, the net mass decrease for the ligand-exchange reaction is 103.39 amu. The mass decrease of $-80 \text{ ng}/(\text{cm}^2 \text{ cycle})$ is equivalent to the loss of $4.66 \times 10^{14} \text{ ZnF}_2 \text{ units}/\text{cm}^2$. This represents the loss of 77% of the ZnF₂ units created on the ZnO surface by the fluorination reaction. The

gain and loss are not equal because other species may be involved in eqs 3, 4. For example, there may be $-\text{CH}_3$ groups on the surface after the TMG reaction and adsorbed HF on the surface after the HF reaction.

Figure 3 shows ΔM_{HF} , ΔM_{TMG} , and the MCPC, defined as $\text{MCPC} = \Delta M_{\text{HF}} + \Delta M_{\text{TMG}}$, for each precursor exposure during

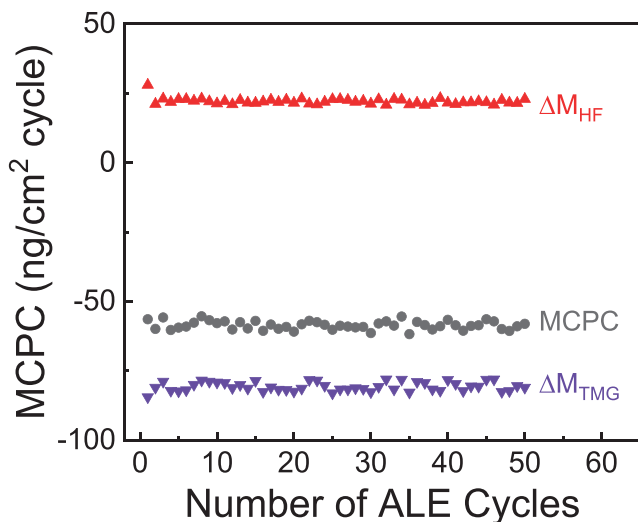


Figure 3. Mass changes for individual HF exposures (ΔM_{HF}), TMG exposures (ΔM_{TMG}), and total mass change per cycle (MCPC) during 50 cycles of ZnO ALE at 100 °C.

the 50 ALE cycles. The ΔM_{HF} , ΔM_{TMG} , and MCPC values were constant throughout the 50 ALE cycles at +22, -80, and -58 ng/cm^2 , respectively, with negligible deviations. The consistent MCPC values yield a constant etch rate for ZnO ALE using HF and TMG.

To confirm the self-limiting behavior during ZnO ALE using HF and TMG as the reactants, the mass changes for each precursor were monitored as a function of exposure. Figure 4 shows the MCPC of ZnO ALE versus the HF and TMG exposures. Figure 4a shows the MCPC values for different HF exposures. The MCPC saturated at -58 ng/cm^2 when the HF exposure was ≥ 200 mTorr·s. In Figure 4b, the MCPC leveled off at -58 ng/cm^2 when the TMG exposure was ≥ 600 mTorr·s.

The MCPC saturation values are consistent with self-limiting HF and TMG reactions during ZnO ALE. The HF reaction is self-limiting because ZnF_2 forms on the ZnO surface and serves as a diffusion barrier for the further fluorination of the underlying ZnO film. The TMG reaction is self-limiting because the ZnF_2 layer is finite and is consumed by the ligand-exchange reaction.

III.II. Ex Situ SE and XRR Measurements. Figure 5 shows the ZnO thickness changes versus number of ALE cycles determined by ex situ SE and XRR measurements at 100 °C. The ZnO thickness changes determined by ellipsometry after 10, 30, 50, 75, and 100 ALE cycles at 100 °C were -10, -26, -46, -78, and -98 Å, respectively. XRR analysis also measured thickness changes of -12, -50, and -102 Å after 10, 50, and 100 ALE cycles at 100 °C. In good agreement with the in situ QCM measurements, the etch rate during ZnO ALE at 100 °C obtained by ex situ SE and XRR measurements was 0.98 Å/cycle.

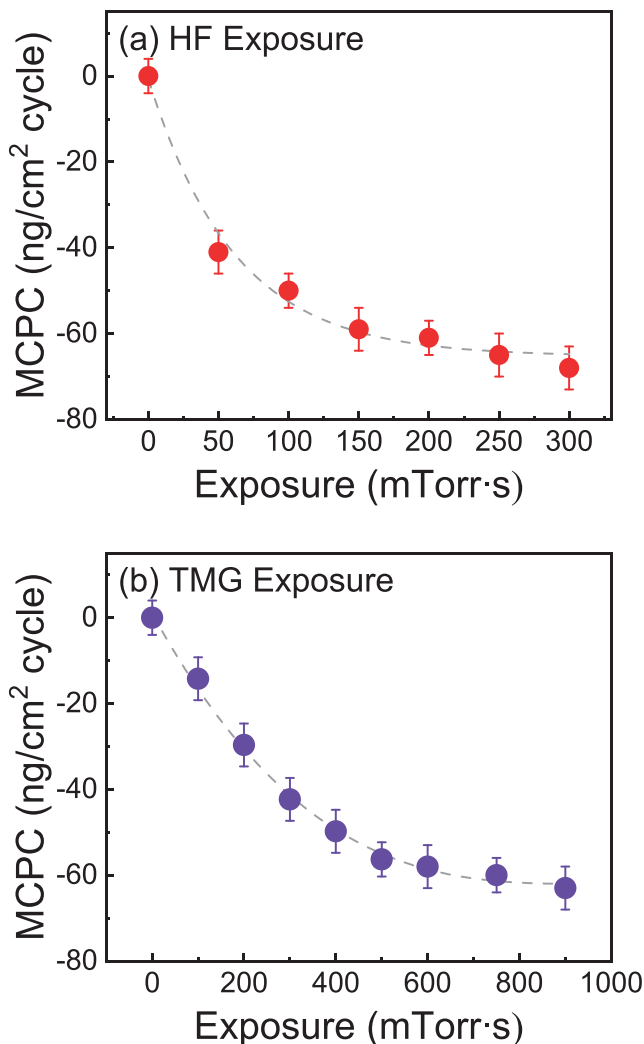


Figure 4. Mass change per cycle (MCPC) versus (a) HF exposure and (b) TMG exposure during ZnO ALE at 100 °C.

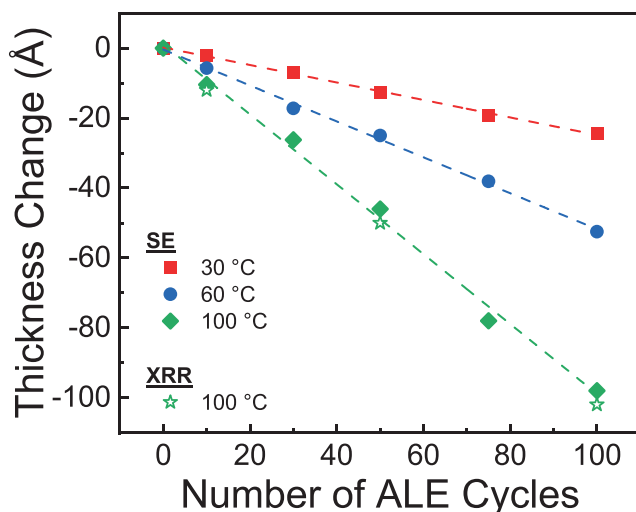


Figure 5. Thickness changes for ZnO versus number of ALE cycles at 30, 60, and 100 °C measured by SE and XRR.

Figure 5 also shows ZnO etching at lower temperatures of 30 and 60 °C using SE. The ZnO etch rates were 0.24 and 0.52

Å/cycle, at 30 and 60 °C, respectively. There is a very broad process temperature range for ZnO ALE using HF and TMG. No other thermal ALE process has been able to etch at temperatures as low as 30 °C. The ability to etch ZnO at temperatures as low as 30 °C indicates that GaF₃ ALD does not compete with ZnO ALE. GaF₃ ALD could occur resulting from sequential HF and TMG exposures in similarity with the ALD of other metal fluorides.²⁹ In comparison, ZnO ALE using sequential HF and TMA exposures could only be performed at temperatures as low as 205 °C because of competing AlF₃ ALD at lower temperatures.^{16,30,31}

Figure 6 displays the etch rates for ZnO ALE over a wide range of temperatures from 30 to 300 °C obtained using ex situ

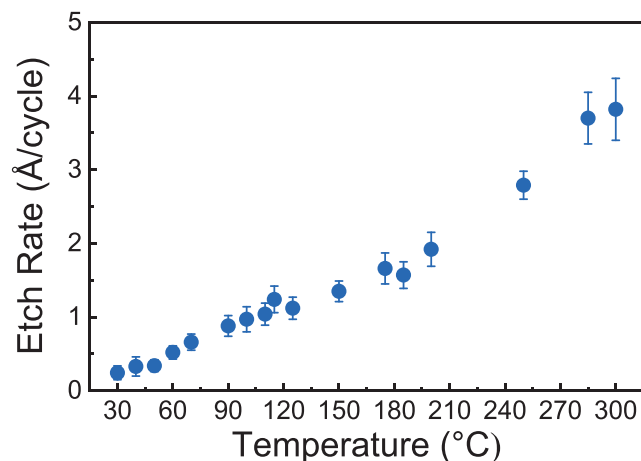


Figure 6. Etch rate of ZnO ALE versus temperature from 30 to 300 °C obtained by ex situ SE measurements.

SE measurements. Some selected etch rates for ZnO using sequential HF and TMG exposures at 30, 60, 90, 150, 200, 250, and 300 °C are 0.24, 0.52, 0.88, 1.35, 1.92, 2.79, and 3.82 Å/cycle, respectively. Like many other thermal ALE processes,^{4,7,13–15,22,32–35} ZnO ALE using HF and TMG is a thermally activated process.

The Arrhenius plot shown in Figure 7 characterizes the temperature dependence from the etch rates in Figure 6 at different temperatures. The Arrhenius analysis of these MCPC values yields an activation barrier of $E_a = 3.3$ kcal/mol from 30 to 300 °C. This activation barrier may reflect the temperature dependence of the underlying fluorination and ligand-exchange reactions. Alternatively, the activation barrier may express the competition between ZnO ALE and GaF₃ ALD in similarity to the competition between Al₂O₃ ALE and AlF₃ ALD during sequential HF and TMA exposures.^{30,31}

III.III. Comparison between TMA or TMG for Thermal ZnO ALE. Additional QCM investigations were performed to demonstrate that TMA converts the ZnO surface to Al₂O₃ and TMG does not convert the ZnO surface. For these experiments, ZnO ALD films were deposited on the QCM sensor. Subsequently, these ZnO ALD films were exposed to TMA or TMG. Figure 8 shows the mass changes during TMA or TMG exposures on ZnO ALD films at 100 °C. In Figure 8a, a rapid mass decrease of $\Delta M_{\text{TMA}} = -92.8$ ng/cm² was observed during the TMA exposure. This mass decrease is consistent with the conversion of ZnO to Al₂O₃.¹²

According to eq 1, the net mass loss is -142.2 amu for the conversion of ZnO to Al₂O₃. The mass decrease of $\Delta M_{\text{TMA}} =$

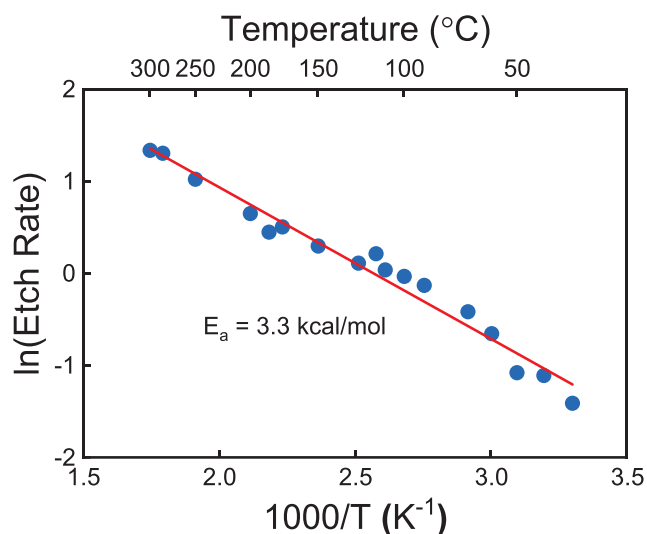


Figure 7. Arrhenius plot showing $\ln(\text{etch rate})$ versus $1000/T$ for etch rates presented in Figure 6. Slope of Arrhenius plot yields an activation barrier of $E_a = 3.3$ kcal/mol.

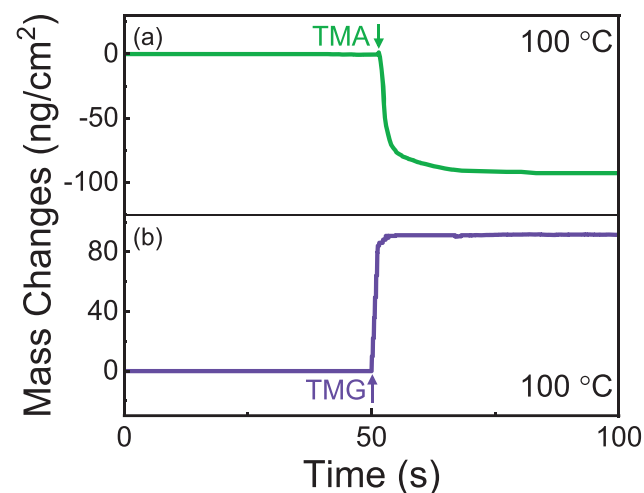


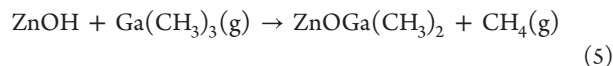
Figure 8. Mass changes during (a) TMA exposure and (b) TMG exposure on a fresh as-deposited ZnO ALD film at 100 °C.

-92.8 ng/cm² can then be equated to 3.93×10^{14} Al₂O₃ units/cm² produced by the conversion reaction. Based on the Al₂O₃ molar mass of 101.96 g/mol and an amorphous Al₂O₃ density of 3.1 g/cm³, these 3.93×10^{14} Al₂O₃ units/cm² represent an Al₂O₃ conversion layer thickness of 2.15 Å formed on the ZnO surface.

HF can then fluorinate the Al₂O₃ conversion layer on ZnO. HF can also adsorb on the fluorinated Al₂O₃ surface at lower temperatures.^{29–31} In particular, previous QCM studies of AlF₃ ALD using HF and TMA have shown that HF is adsorbed on the AlF₃ surface after the HF exposure at 150 °C.^{29,30} The mass changes from QCM analysis are consistent with an HF coverage of 0.8 HF molecule for every AlF₃ unit deposited during one AlF₃ ALD cycle.²⁹ The adsorbed HF is then available to react with the next TMA exposure to form AlF₃. This AlF₃ ALD reaction between HF and TMA prevents Al₂O₃ etching using sequential HF and TMA exposures at lower temperatures $T < 205$ °C.^{16,29–31}

In contrast to the pronounced mass loss observed for the TMA reaction with ZnO, Figure 8b shows that a mass increase

of $\Delta M_{\text{TMG}} = 91.63 \text{ ng/cm}^2$ was observed during TMG exposure to ZnO. This mass increase is consistent with the adsorption of TMG on the ZnO surface. This TMG adsorption on ZnOH surface species may occur as



From eq 5, the net mass increase is 98.78 amu. The mass increase of $\Delta M_{\text{TMG}} = 91.63 \text{ ng/cm}^2$ can then be equated to $5.6 \times 10^{14} \text{ Ga}(\text{CH}_3)_2$ units/cm² produced by the adsorption of TMG on ZnOH surface species. HF exposures on the ZnO surface after TMG adsorption may then lead to the release of $\text{GaF}_x(\text{CH}_3)_y$ species and H₂O from HF fluorination of ZnO.

The conversion of ZnO to Al₂O₃ by TMA could lead to impurities remaining in the ZnO film after etching. To identify impurity elements, XPS was performed after 50 cycles of ZnO ALE at 250 °C using either HF/TMA or HF/TMG exposures. The last precursor exposure for each experiment was either TMA or TMG. The XPS measurements were performed without any prior Ar⁺ sputtering. These XPS survey spectra are given in Figure S1, Supporting Information. When ZnO was etched using HF/TMA exposures, the F and Al XPS signals were 8.3 and 7.8 at. %, respectively. In contrast, when ZnO was etched using HF/TMG exposures, the F and Ga XPS signals were 0.4 and 2.6 at. %, respectively. A table of the main atomic concentrations from the XPS survey spectra are presented in Table S1, Supporting Information.

The XPS results reveal that the conversion of ZnO to Al₂O₃ by TMA leads to the incorporation of Al and F in the ZnO film. The high F levels of 8.3 at. % after etching using HF and TMA exposures are believed to result from the residual Al complexing F in the ZnO film. In contrast, for ZnO ALE using HF and TMG exposures, the Ga and F levels are consistent with only surface adsorption.

III.IV. Mass Spectrometry Studies of Thermal ZnO ALE. QMS experiments were performed to monitor ZnO ALE using sequential HF and TMG exposures at 100 °C. Figure 9 shows the ion signal intensities during TMG exposures on fresh ZnO powder. Figure 9a reveals the ion signal intensities from *m/z* 5 to 40. Signals in this range are attributed to methyl (CH₃⁺) and other fragments from the Ga(CH₃)₃⁺ parent. Figure 9b displays the ion signal intensities from *m/z* 60 to 120 that are attributed to the Ga(CH₃)₃⁺ parent and its fragments. The dominant ion signals are observed at *m/z* 99 and 101. These ion signals correspond to Ga(CH₃)₂⁺ and the expected intensity distribution based on the natural isotopic abundances. Gallium has two stable isotopes: ⁶⁹Ga (60.10%) and ⁷¹Ga (39.90%).³⁶

There is no evidence from the mass spectra in Figure 9 for any conversion of ZnO to Ga₂O₃ at 100 °C. If TMG was able to convert ZnO to Ga₂O₃, then Zn(CH₃)₂ would be the expected reaction product.¹² However, no indication of Zn(CH₃)₂ is observed in Figure 9b. The production of Zn(CH₃)₂ would lead to the observation of Zn(CH₃)₂⁺ at *m/z* 94 and Zn(CH₃)⁺ at *m/z* 79. Neither of these ion signals are monitored during the TMG exposure. The absence of these ion signals argues against the conversion of ZnO to Ga₂O₃ by TMG.

Figure 10 shows the volatile products formed during the TMG exposure on fluorinated ZnO during the fifth ALE cycle at 100 °C over three different mass ranges. In Figure 10a for *m/z* 102 to 110, signals at *m/z* 103 and 105 correspond to GaF(CH₃)⁺ and its isotopes. GaF(CH₃)₂ is the expected

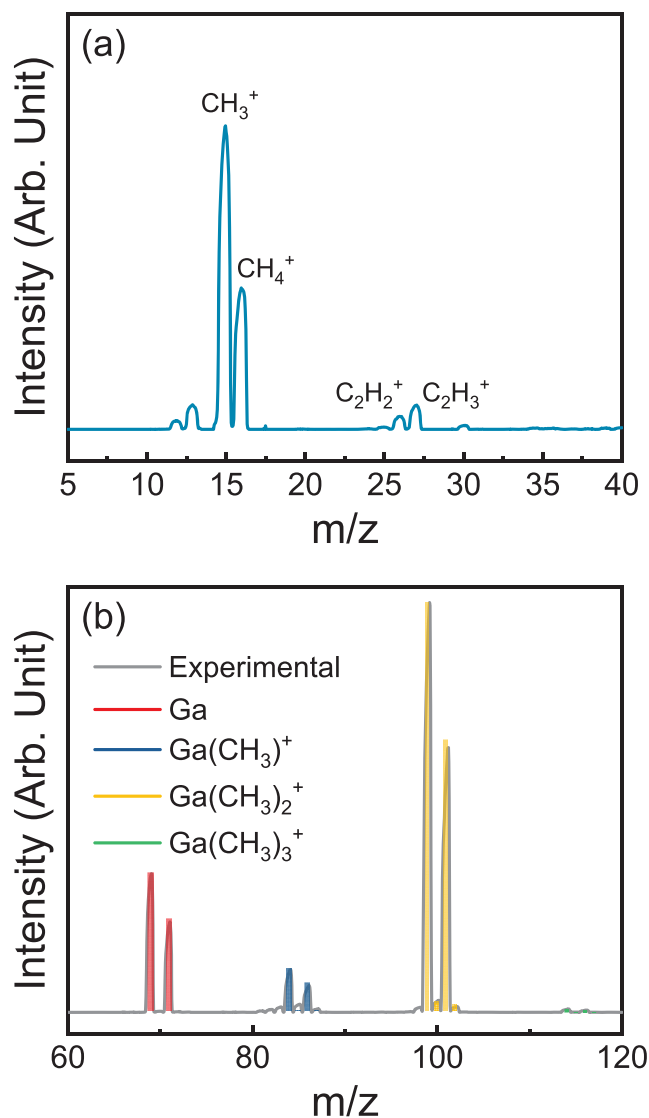


Figure 9. QMS spectra during first TMG exposure to ZnO powder at 100 °C in two different spectral regions: (a) *m/z* 5 to 40, and (b) *m/z* 60 to 120.

product from the ligand-exchange reaction given by eq 4. In addition to the monomer ligand-exchange products, Ga dimers are also observed as etch products. In Figure 10b for *m/z* 215 to 230, signals at *m/z* 217, 219, 221, 223, and 225 are consistent with the dimers Ga₂F(CH₃)₄⁺, Ga₂F₂(CH₃)₃⁺, and their isotopes.

Zn(CH₃)₂ is also observed as an etch product during the TMG exposure. Zn(CH₃)⁺ is the main ion signal observed from the ionization of Zn(CH₃)₂. Figure 10c shows this ion signal for Zn(CH₃)⁺ at *m/z* 79. Other weaker peaks from Zn(CH₃)⁺ based on the natural isotopic abundances should be observed at *m/z* 81, 82, and 83. Unfortunately, these peaks overlap with other ion signal intensities in Figure 10c that can be attributed to GaC⁺ at *m/z* 81, GaCH⁺ at *m/z* 82, and GaCH₂⁺ at *m/z* 83.

Figure 11 shows the time-resolved ion signals during sequential TMG and HF exposures on ZnO powder. The first TMG exposure on fresh ZnO powder did not produce an Zn(CH₃)⁺ ion signal at *m/z* 79. The absence of this Zn(CH₃)⁺ ion signal indicates that TMG did not convert ZnO to Ga₂O₃.

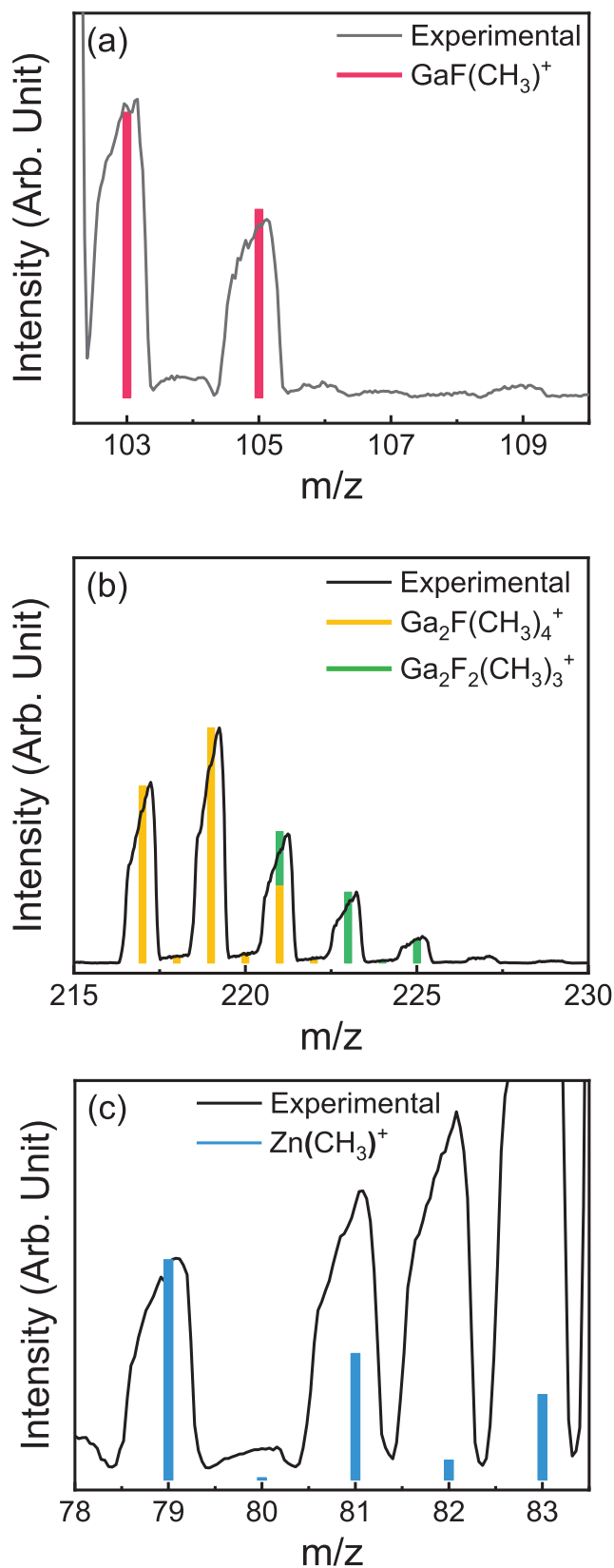


Figure 10. QMS spectra during 5th TMG exposure during 5th ALE cycle on ZnO powder at 100 °C in three different spectral regions: (a) m/z 102 to 110, (b) m/z 215 to 230, and (c) m/z 78 to 84. Expected intensities are also displayed based on natural isotopic abundances.

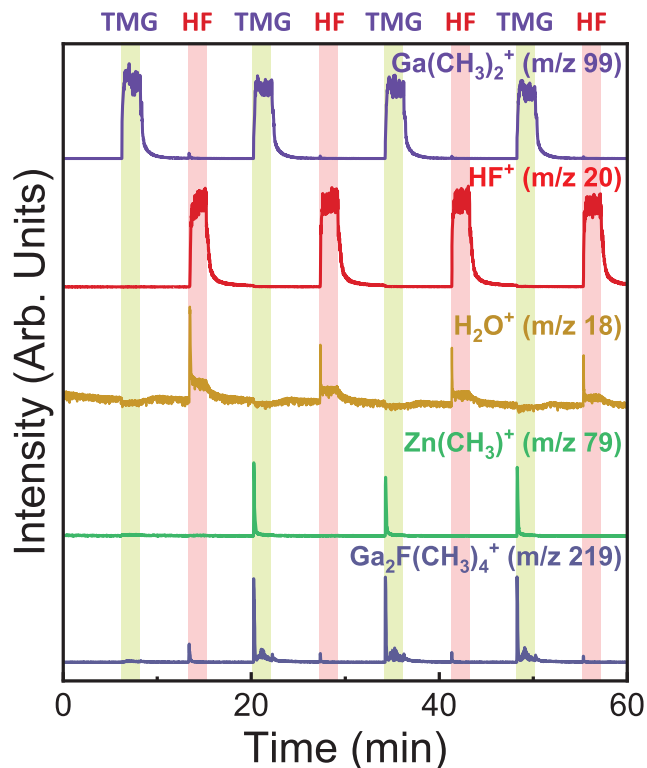


Figure 11. Time-resolved ion signal intensities for $\text{Ga}(\text{CH}_3)_2^+$ at m/z 99, HF^+ at m/z 20, H_2O^+ at m/z 18, $\text{Zn}(\text{CH}_3)^+$ at m/z 79, and $\text{Ga}_2\text{F}(\text{CH}_3)_4^+$ at m/z 219 during ZnO ALE using sequential TMG and HF and exposures on ZnO powder at 100 °C. TMG exposure is indicated by light green-shaded region. HF exposure is designated by light red-shaded region.

Ion signals for $\text{Ga}_2\text{F}(\text{CH}_3)_4^+$ at m/z 219 and H_2O^+ at m/z 20 were then produced during the following HF exposure. The $\text{Ga}_2\text{F}(\text{CH}_3)_4^+$ ion species originate from a Ga dimer species generated by the removal of TMG adsorption products on ZnO. The H_2O^+ ion signal is derived from H_2O formed by the fluorination of ZnO powder according to eq 3.

After the HF exposure, the following TMG exposure produced ion signals for $\text{Zn}(\text{CH}_3)^+$ at m/z 79 and $\text{Ga}_2\text{F}(\text{CH}_3)_4^+$ at m/z 219. The $\text{Ga}_2\text{F}(\text{CH}_3)_4^+$ ion signal results from a Ga dimer species produced by the ligand-exchange reaction between TMG and the fluorinated ZnO surface. The Ga dimer species could be either $\text{Ga}_2\text{F}_2(\text{CH}_3)_4$ or $\text{Ga}_2\text{F}(\text{CH}_3)_5$. The $\text{Zn}(\text{CH}_3)^+$ ion signal is attributed to the $\text{Zn}(\text{CH}_3)_2$ etch product resulting from the ligand-exchange reaction between TMG and the ZnF_2 surface. Additional sequential HF and TMG exposures produce the same reaction products.

The time-dependent ion signal intensities for both $\text{Ga}_2\text{F}(\text{CH}_3)_4^+$ and $\text{Zn}(\text{CH}_3)^+$ increase quickly and then are rapidly reduced to the noise level during the TMG exposure. This behavior is attributed to self-limiting reactions between TMG and the fluorinated ZnO surface. In addition, the $\text{Ga}_2\text{F}(\text{CH}_3)_4^+$ and $\text{Zn}(\text{CH}_3)^+$ ion signal intensities are very consistent between the various TMG exposures. The H_2O^+ ion signal intensities are also very steady during the HF exposures. These unchanging ion signal intensities for the etch products are in agreement with a constant etch rate during the sequential TMG and HF exposures. There is also a small $\text{Ga}_2\text{F}(\text{CH}_3)_4^+$ ion signal during the HF exposures. This $\text{Ga}_2\text{F}(\text{CH}_3)_4^+$ ion

signal indicates that HF exposures can displace TMG adsorption products on the surface from the TMG exposure.

The time-evolution of ion signal intensities for $\text{Ga}_2\text{F}(\text{CH}_3)_4^+$ at m/z 219, H_2O^+ at m/z 18, and HF^+ at m/z 20 during the first HF exposure is shown in Figure 12. These results reveal

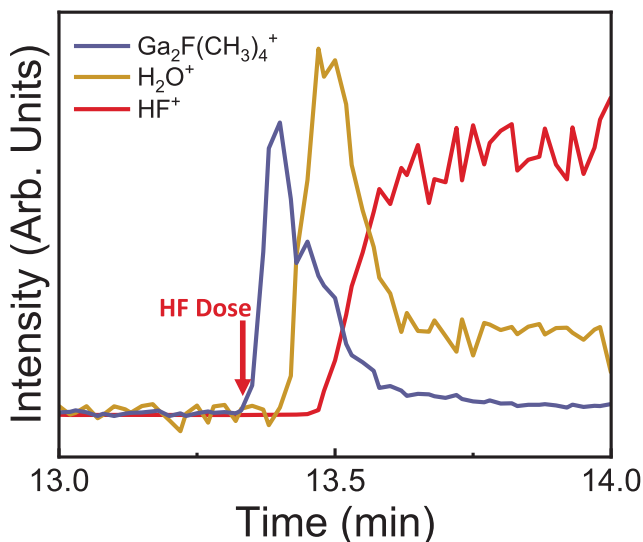


Figure 12. Time-resolved ion signal intensities for $\text{Ga}_2\text{F}(\text{CH}_3)_4^+$ at m/z 219, H_2O^+ at m/z 18, and HF^+ at m/z 20 during first HF exposure on ZnO powder after first TMG exposure.

the sequential nature of the reactions within the first HF exposure after the first TMG exposure. The $\text{Ga}_2\text{F}(\text{CH}_3)_4^+$ ion signal results from Ga dimer species produced by HF reaction with TMG adsorption species on the ZnO surface. After the TMG adsorption species are removed, HF fluorinates the ZnO surface to ZnF_2 and releases H_2O . After the ZnO fluorination, the HF reactant can then pass through the ZnO powder without any reaction.

III.V. Etch Rates of Various Metal Oxides Using Sequential HF and TMG Exposures. Figure 13 displays the etching of ZnO, Al_2O_3 , ZrO_2 , and HfO_2 using sequential

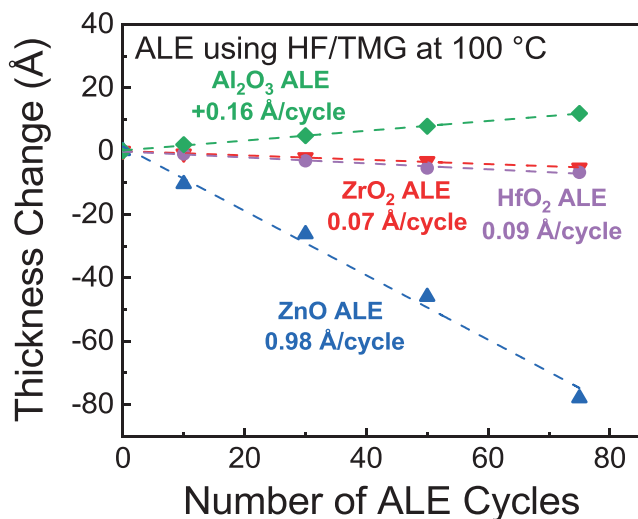


Figure 13. Thickness changes of Al_2O_3 , ZrO_2 , HfO_2 , and ZnO films measured by ex situ SE as a function of ALE cycles using sequential HF and TMG exposures at 100 °C.

HF and TMG exposures at 100 °C measured by ex situ SE. Compared with the etch rate for ZnO ALE at 0.98 Å/cycle, the etch rates for ZrO_2 and HfO_2 ALE at 100 °C were much smaller at 0.07 and 0.09 Å/cycle, respectively. Al_2O_3 did not etch versus HF and TMG exposures. The sequential HF and TMG exposures led to a film growth of 0.16 Å/cycle using the ellipsometry model for a ZnO film.

This different behavior for the various metal oxides can be explained by the Lewis acidity of the corresponding metal fluorides. The Lewis acidity will determine the HF adsorption on the metal fluorides.²⁹ If HF adsorbs on the metal fluorides, then the TMG may interact with the adsorbed HF instead of the underlying metal fluoride. This interaction may form a gallium fluoride complex that may prevent the ligand-exchange reaction with the underlying metal fluoride that is needed for etching.

Figure 13 shows that ZnO etches easily at 100 °C. ZnO is fluorinated by HF to form ZnF_2 during ZnO ALE using sequential HF and TMG exposures. ZnF_2 is a weak Lewis acid. ZnF_2 does not readily adsorb HF on its surface. Earlier QCM studies have shown that no HF adsorbs on the ZnF_2 surface during ZnF_2 ALD with sequential DEZ and HF exposures at 150 °C.²⁹ With no HF on the ZnF_2 surface, TMG is able to undergo ligand-exchange reactions with the ZnF_2 surface at temperatures as low as 30 °C.

The lack of HF adsorption on the ZnF_2 surface after HF exposures also does not allow TMG to react with adsorbed HF to produce GaF_3 or $\text{GaF}_x(\text{CH}_3)_y$ surface complexes. If these GaF_3 or $\text{GaF}_x(\text{CH}_3)_y$ surface complexes were formed, then they could react with the next HF exposure to form a GaF_3 layer on the ZnF_2 surface. The GaF_3 layer may also contain additional adsorbed HF. The GaF_3 layer with adsorbed HF could then react with the next TMG exposure to form additional GaF_3 or $\text{GaF}_x(\text{CH}_3)_y$ surface complexes. The subsequent HF and TMG sequential exposures could then lead to GaF_3 ALD similar to AlF_3 ALD using sequential HF and TMA exposures at low temperatures.³⁰ ZnO etching with no indication of any film growth argues against GaF_3 ALD from sequential HF and TMG exposures.

The Lewis acidity of the various metal fluoride surfaces may also explain the lower etch rates for ZrO_2 and HfO_2 ALE using HF and TMG at 100 °C shown in Figure 13. ZrF_4 and HfF_4 have intermediate Lewis acidities as measured by the QCM studies of HF adsorption on metal fluoride surfaces at 150 °C.²⁹ These intermediate Lewis acidities may lead to partial HF coverages that reduce but do not completely prevent the ZrO_2 and HfO_2 ALE.

The slight thickness increase observed on Al_2O_3 during the sequential HF and TMG exposures in Figure 13 could be also explained by the Lewis acidity of the Al_2O_3 surface. The fluorination of Al_2O_3 produces an AlF_3 surface layer. AlF_3 is a strong Lewis acid that can adsorb HF.^{29–31} This adsorbed HF is known to react with TMA and produce AlF_3 ALD using sequential HF and TMA exposures at $T < 250$ °C.^{30,31} The adsorbed HF on AlF_3 may also react with TMG and lead to GaF_3 formation during sequential HF and TMG exposures on Al_2O_3 at 100 °C.

III.VI. ZnO Surface Roughness versus ALE Cycles. The ability of ZnO ALE to smooth the ZnO surface was explored at 100 °C. AFM images of the original ZnO surface and after 25, 50, 75, and 100 ZnO ALE cycles at 100 °C are shown in Figure S2, Supporting Information. Figure 14 shows the RMS roughness of an initial ZnO ALD film as a function of ZnO

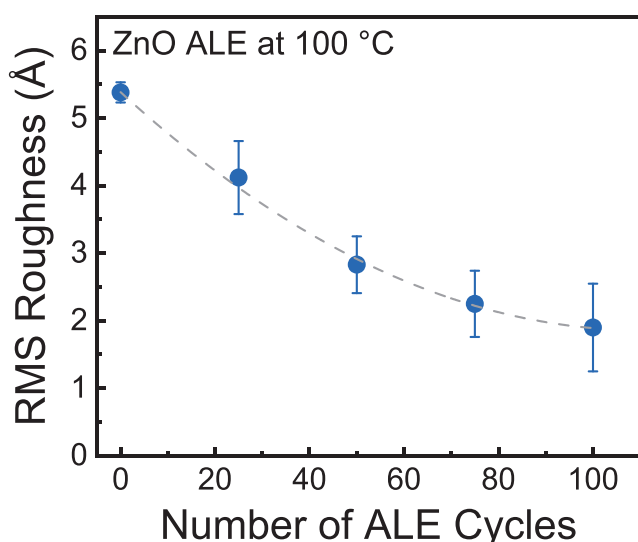


Figure 14. RMS roughness of initial ZnO ALD film measured by AFM versus number of ZnO ALE cycles at 100 °C.

ALE cycles using sequential HF and TMG exposures. The RMS roughness of the initial as-grown ZnO ALD film was 5.4 Å. The RMS values decreased to 4.1, 2.8, 2.3, and 1.9 Å after 25, 50, 75, and 100 ALE cycles, respectively. Similar surface smoothing has been observed in previous ALE studies on Al_2O_3 ,^{33,37,38} HfO_2 ,³⁹ Si_3N_4 ,³² GaN ,⁴⁰ and SiO_2 .⁴¹ The ability of thermal ALE to smooth surfaces can be explained by isotropic etching and curvature dependent surface fluorination.^{38,42–44}

IV. CONCLUSIONS

ZnO thermal atomic ALE was observed over a wide temperature range from 30 to 300 °C using sequential exposures of HF and TMG. Stepwise mass increases during HF exposures and larger mass decreases during TMG exposures were observed by QCM studies. The mass changes per cycle were self-limiting as a function of HF and TMG exposures at 100 °C. Etch rates for ZnO thermal ALE were measured over a wide temperature range using spectroscopic ellipsometry. ZnO thermal ALE could be observed at temperatures as low as 30 °C. The ZnO etch rates ranged from 0.24 Å/cycle at 30 °C to 3.82 Å/cycle at 300 °C. An Arrhenius analysis of the temperature-dependent etch rates yielded an activation barrier of $E_a = 3.3$ kcal/mol.

Although the HF and TMG precursors could lead to either ZnO thermal ALE or GaF_3 ALD, there is no competing GaF_3 ALD that interferes with the ZnO thermal ALE. The ability to etch ZnO at low temperatures was attributed to this lack of GaF_3 ALD. In addition, TMG did not convert ZnO to Ga_2O_3 . ZnO thermal ALE was able to proceed according to fluorination of ZnO to ZnF_2 by HF and then removal of ZnF_2 by the TMG ligand-exchange reaction. In contrast, earlier studies of ZnO thermal ALE using sequential exposures of HF and TMA observed the conversion of ZnO to Al_2O_3 by TMA. After conversion to Al_2O_3 , HF is able to adsorb on the fluorinated Al_2O_3 surface. The adsorbed HF then leads to AlF_3 ALD during the subsequent TMA exposure. The competing AlF_3 ALD limits the lower temperature for ZnO thermal ALE using HF and TMA exposures.

The ability of TMG and TMA exposures to convert ZnO was explored by QCM and QMS studies. QCM studies

compared TMG and TMA exposures at 100 °C on fresh ZnO surfaces grown by ZnO ALD. The TMG exposures led to a mass gain that was attributed to TMG adsorption on the ZnO surface. In contrast, TMA exposures produced a pronounced mass loss that was consistent with the conversion of ZnO to Al_2O_3 . QMS analysis also did not observe the possible $\text{Zn}(\text{CH}_3)_2$ conversion product during the first TMG exposure on ZnO. The ion signals observed during sequential HF and TMG exposures were consistent with fluorination of ZnO to ZnF_2 by HF and then ligand-exchange between TMG and ZnF_2 to produce $\text{Zn}(\text{CH}_3)_2$ and $\text{GaF}(\text{CH}_3)_2$ etch products.

The sequential HF and TMG exposures were observed to be selective for ZnO ALE compared with HfO_2 , ZrO_2 or Al_2O_3 ALE. The selectivity was explained by the Lewis acidity of the corresponding metal fluorides. ZnF_2 is a weak Lewis acid that does not readily adsorb HF on its surface. Without HF on the ZnF_2 surface, TMG can undergo ligand-exchange with ZnF_2 instead of reacting with HF. ZnO surfaces were also smoothed progressively versus number of ZnO ALE cycles.

■ ASSOCIATED CONTENT

Supporting Information

The Supporting Information is available free of charge at <https://pubs.acs.org/doi/10.1021/acs.chemmater.5c00028>.

XPS survey spectra of ZnO after ALE; table of main atomic concentrations from the XPS survey spectra; and AFM images of original ZnO surface and after ZnO ALE (PDF)

■ AUTHOR INFORMATION

Corresponding Author

Steven M. George – Department of Chemistry, University of Colorado, Boulder, Colorado 80309, United States;

orcid.org/0000-0003-0253-9184;

Email: Steven.George@Colorado.edu

Authors

Taewook Nam – Department of Chemistry, University of Colorado, Boulder, Colorado 80309, United States; Department of Semiconductor Systems Engineering, Sejong University, Gwangjin-Gu, Seoul 05006, Republic of Korea; Institute of Semiconductor and System IC, Sejong University, Gwangjin-Gu, Seoul 05006, Republic of Korea; orcid.org/0000-0001-9702-0873

David R. Zywojtko – Department of Chemistry, University of Colorado, Boulder, Colorado 80309, United States

Troy A. Colleran – Department of Chemistry, University of Colorado, Boulder, Colorado 80309, United States

Jonathan L. Partridge – Department of Chemistry, University of Colorado, Boulder, Colorado 80309, United States; orcid.org/0000-0002-0071-9854

Complete contact information is available at: <https://pubs.acs.org/doi/10.1021/acs.chemmater.5c00028>

Author Contributions

^{||}T.N. and D.R.Z. contributed equally to this work.

Notes

The authors declare no competing financial interest.

■ ACKNOWLEDGMENTS

This work was funded by Tokyo Electron and by the faculty research fund of Sejong University in 2024. Additional support

was supplied by the Joint University Microelectronics Program (JUMP) funded by the Semiconductor Research Corporation (SRC). Funding for the QMS reactor and the QMS investigations was provided by Lam Research. The authors thank Dr. Jessica Murdzek for the XRR measurements and Dr. Andrew Cavanagh for the XPS measurements.

REFERENCES

- (1) T Carver, C.; Plombon, J. J.; Romero, P. E.; Suri, S.; Tronic, T. A.; Turkot, R. B. Atomic Layer Etching: An Industry Perspective. *ECS J. Solid State Sci. Technol.* **2015**, *4*, N5005–N5009.
- (2) George, S. M. Mechanisms of Thermal Atomic Layer Etching. *Acc. Chem. Res.* **2020**, *53*, 1151–1160.
- (3) Kanarik, K. J.; Lill, T.; Hudson, E. A.; Sriraman, S.; Tan, S.; Marks, J.; Vahedi, V.; Gottscho, R. A. Overview of Atomic Layer Etching in the Semiconductor Industry. *J. Vac. Sci. Technol., A* **2015**, *33*, No. 020802.
- (4) George, S. M.; Lee, Y. Prospects for Thermal Atomic Layer Etching Using Sequential, Self-Limiting Fluorination and Ligand-Exchange Reactions. *ACS Nano* **2016**, *10*, 4889–4894.
- (5) Fischer, A.; Routzahn, A.; George, S. M.; Lill, T. Thermal Atomic Layer Etching: A Review. *J. Vac. Sci. Technol., A* **2021**, *39*, No. 030801.
- (6) Lee, Y.; DuMont, J. W.; George, S. M. Trimethylaluminum as the Metal Precursor for the Atomic Layer Etching of Al₂O₃ Using Sequential, Self-Limiting Thermal Reactions. *Chem. Mater.* **2016**, *28*, 2994–3003.
- (7) Reif, J.; Knaut, M.; Killge, S.; Albert, M.; Mikolajick, T.; Bartha, J. W. In Situ Studies on Atomic Layer Etching of Aluminum Oxide Using Sequential Reactions with Trimethylaluminum and Hydrogen Fluoride. *J. Vac. Sci. Technol., A* **2022**, *40*, No. 032602.
- (8) Kondati Natarajan, S.; Elliott, S. D. Modeling the Chemical Mechanism of the Thermal Atomic Layer Etch of Aluminum Oxide: A Density Functional Theory Study of Reactions during HF Exposure. *Chem. Mater.* **2018**, *30*, 5912–5922.
- (9) Clancey, J. W.; Cavanagh, A. S.; Smith, J. E. T.; Sharma, S.; George, S. M. Volatile Etch Species Produced during Thermal Al₂O₃ Atomic Layer Etching. *J. Phys. Chem. C* **2020**, *124*, 287–299.
- (10) Lii-Rosales, A.; Cavanagh, A. S.; Fischer, A.; Lill, T.; George, S. M. Spontaneous Etching of Metal Fluorides Using Ligand-Exchange Reactions: Landscape Revealed by Mass Spectrometry. *Chem. Mater.* **2021**, *33*, 7719–7730.
- (11) Hu, X.; Schuster, J. Chemical Mechanism of AlF₃ Etching during AlMe₃ Exposure: A Thermodynamic and DFT Study. *J. Phys. Chem. C* **2022**, *126*, 7410–7420.
- (12) Myers, T. J.; Cano, A. M.; Lancaster, D. K.; Clancey, J. W.; George, S. M. Conversion Reactions in Atomic Layer Processing with Emphasis on ZnO Conversion to Al₂O₃ by Trimethylaluminum. *J. Vac. Sci. Technol., A* **2021**, *39*, No. 021001.
- (13) Johnson, N. R.; George, S. M. WO₃ and W Thermal Atomic Layer Etching Using “Conversion-Fluorination” and “Oxidation-Conversion-Fluorination” Mechanisms. *ACS Appl. Mater. Interfaces* **2017**, *9*, 34435–34447.
- (14) Cano, A. M.; Partridge, J. L.; George, S. M. Thermal Atomic Layer Etching of Al₂O₃ Using Sequential HF and BCl₃ Exposures: Evidence for Combined Ligand-Exchange and Conversion Mechanisms. *Chem. Mater.* **2022**, *34*, 6440–6449.
- (15) Nam, T.; Partridge, J. L.; George, S. M. Thermal Atomic Layer Etching of Zinc Sulfide Using Sequential Trimethylaluminum and Hydrogen Fluoride Exposures: Evidence for a Conversion Mechanism. *Chem. Mater.* **2023**, *35*, 6671–6681.
- (16) Zywotko, D. R.; George, S. M. Thermal Atomic Layer Etching of ZnO by a “Conversion-Etch” Mechanism Using Sequential Exposures of Hydrogen Fluoride and Trimethylaluminum. *Chem. Mater.* **2017**, *29*, 1183–1191.
- (17) Roine, A. *HSC Chemistry 9.9.2.3*; Outokumpu Research Oy: Pori, Finland, 2019.
- (18) Marnett, A.; Verheijen, M. A.; Mackus, A. J. M.; Kessels, W. M. M.; Roozeboom, F. Isotropic Atomic Layer Etching of ZnO Using Acetylacetone and O₂ Plasma. *ACS Appl. Mater. Interfaces* **2018**, *10*, 38588–38595.
- (19) Gaskill, D. K.; Bottka, N.; Lin, M.-C. Growth of GaN Films Using Trimethylgallium and Hydrazine. *Appl. Phys. Lett.* **1986**, *48*, 1449–1451.
- (20) Bhat, R.; Koza, M.; Skromme, B. Growth of High-Quality GaAs Using Trimethylgallium and Diethylarsine. *Appl. Phys. Lett.* **1987**, *50*, 1194–1196.
- (21) Hatch, K. A.; Messina, D. C.; Nemanich, R. J. Plasma Enhanced Atomic Layer Deposition and Atomic Layer Etching of Gallium Oxide Using Trimethylgallium. *J. Vac. Sci. Technol., A* **2022**, *40*, No. 042603.
- (22) Lee, Y.; Johnson, N. R.; George, S. M. Thermal Atomic Layer Etching of Gallium Oxide Using Sequential Exposures of HF and Various Metal Precursors. *Chem. Mater.* **2020**, *32*, 5937–5948.
- (23) Cho, I.; Shong, B. Exchange Reactions during Atomic Layer Deposition of Ternary Group 13 Oxides and Nitrides. *ACS Appl. Electron. Mater.* **2024**, *6*, 7495–7502.
- (24) Elam, J. W.; Groner, M. D.; George, S. M. Viscous Flow Reactor with Quartz Crystal Microbalance for Thin Film Growth by Atomic Layer Deposition. *Rev. Sci. Instrum.* **2002**, *73*, 2981–2987.
- (25) Partridge, J. L.; Murdzek, J. A.; Johnson, V. L.; Cavanagh, A. S.; Fischer, A.; Lill, T.; Sharma, S.; George, S. M. Thermal Atomic Layer Etching of CoO, ZnO, Fe₂O₃, and NiO by Chlorination and Ligand Addition Using SO₂Cl₂ and Tetramethylethylenediamine. *Chem. Mater.* **2023**, *35*, 2058–2068.
- (26) Murdzek, J. A.; George, S. M. Effect of Crystallinity on Thermal Atomic Layer Etching of Hafnium Oxide, Zirconium Oxide, and Hafnium Zirconium Oxide. *J. Vac. Sci. Technol., A* **2020**, *38*, No. 022608.
- (27) Wagner, C. D.; Muilenberg, G. E. *Handbook of X-ray Photoelectron Spectroscopy: A Reference Book of Standard Data for Use in X-ray Photoelectron Spectroscopy*; Perkin-Elmer, 1979.
- (28) Major, G. H.; Fairley, N.; Sherwood, P. M. A.; Linford, M. R.; Terry, J.; Fernandez, V.; Artyushkova, K. Practical Guide for Curve Fitting in X-Ray Photoelectron Spectroscopy. *J. Vac. Sci. Technol., A* **2020**, *38*, No. 061203.
- (29) Lee, Y.; Sun, H.; Young, M. J.; George, S. M. Atomic Layer Deposition of Metal Fluorides Using HF–Pyridine as the Fluorine Precursor. *Chem. Mater.* **2016**, *28*, 2022–2032.
- (30) Lee, Y.; DuMont, J. W.; Cavanagh, A. S.; George, S. M. Atomic Layer Deposition of AlF₃ Using Trimethylaluminum and Hydrogen Fluoride. *J. Phys. Chem. C* **2015**, *119*, 14185–14194.
- (31) DuMont, J. W.; George, S. M. Competition between Al₂O₃ Atomic Layer Etching and AlF₃ Atomic Layer Deposition Using Sequential Exposures of Trimethylaluminum and Hydrogen Fluoride. *J. Chem. Phys.* **2017**, *146*, No. 052819.
- (32) Abdulagatov, A. I.; George, S. M. Thermal Atomic Layer Etching of Silicon Nitride Using an Oxidation and “Conversion Etch” Mechanism. *J. Vac. Sci. Technol., A* **2020**, *38*, No. 022607.
- (33) Lee, Y.; George, S. M. Thermal Atomic Layer Etching of Al₂O₃, HfO₂, and ZrO₂ Using Sequential Hydrogen Fluoride and Dimethylaluminum Chloride Exposures. *J. Phys. Chem. C* **2019**, *123*, 18455–18466.
- (34) Nam, T.; Collieran, T. A.; Partridge, J. L.; Cavanagh, A. S.; George, S. M. Thermal Atomic Layer Etching of Molybdenum Using Sequential Oxidation and Deoxychlorination Reactions. *Chem. Mater.* **2024**, *36*, 1449–1458.
- (35) Xie, W. Y.; Lemaire, P. C.; Parsons, G. N. Thermally Driven Self-Limiting Atomic Layer Etching of Metallic Tungsten Using WF₆ and O₂. *ACS Appl. Mater. Interfaces* **2018**, *10*, 9147–9154.
- (36) Hoefs, J. *Stable Isotope Geochemistry*, 4th ed.; Springer: Berlin Heidelberg, 1997.
- (37) Lee, Y.; George, S. M. Atomic Layer Etching of Al₂O₃ Using Sequential, Self-Limiting Thermal Reactions with Sn(acac)₂ and Hydrogen Fluoride. *ACS Nano* **2015**, *9*, 2061–2070.
- (38) Zywotko, D. R.; Faguet, J.; George, S. M. Rapid Atomic Layer Etching of Al₂O₃ Using Sequential Exposures of Hydrogen Fluoride

and Trimethylaluminum with No Purging. *J. Vac. Sci. Technol., A* **2018**, *36*, No. 061508.

(39) Lee, Y.; DuMont, J. W.; George, S. M. Atomic Layer Etching of HfO₂ Using Sequential, Self-Limiting Thermal Reactions with Sn(acac)₂ and HF. *ECS J. Solid State Sci. Technol.* **2015**, *4*, N5013–N5022.

(40) Chittock, N. J.; Shu, Y.; Elliott, S. D.; Knoops, H. C. M.; Kessels, W. M. M.; Mackus, A. J. M. Isotropic atomic layer etching of GaN using SF₆ Plasma and Al(CH₃)₃. *J. Appl. Phys.* **2023**, *134*, No. 075302.

(41) Catherall, D. S.; Hossain, A. A.; Ardizzi, A. J.; Minnich, A. J. Atomic Layer Etching of SiO₂ Using Sequential Exposures of Al(CH₃)₃ and H₂/SF₆ Plasma. *J. Vac. Sci. Technol., A* **2024**, *42*, No. 052605.

(42) Gerritsen, S. H.; Chittock, N. J.; Vandalon, V.; Verheijen, M. A.; Knoops, H. C. M.; Kessels, W. M. M.; Mackus, A. J. M. Surface Smoothing by Atomic Layer Deposition and Etching for the Fabrication of Nanodevices. *ACS Appl. Nano Mater.* **2022**, *5*, 18116–18126.

(43) Murdzek, J. A.; Rajashekhar, A.; Makala, R. S.; George, S. M. Thermal Atomic Layer Etching of Amorphous and Crystalline Al₂O₃ Films. *J. Vac. Sci. Technol., A* **2021**, *39*, No. 042602.

(44) Myers, T. J.; Throckmorton, J. A.; Borrelli, R. A.; O'Sullivan, M.; Hatwar, T.; George, S. M. Smoothing Surface Roughness Using Al₂O₃ Atomic Layer Deposition. *Appl. Surf. Sci.* **2021**, *569*, No. 150878.